THE JOURNAL OF PHYSICAL CHEMISTRY C

Article

pubs.acs.org/JPCC

Computational Investigation on Hydrodeoxygenation (HDO) of Acetone to Propylene on α-MoO_3 (010) Surface

Manish Shetty, Beat Buesser,† Yuriy Román-Leshkov, and William H. Green*

Department of Chemical Engineering, Massachusetts Institute of Technology, Cambridge, Massachusetts 02139, United States

Supporting Information

ABSTRACT: Density functional theory (DFT) calculations were performed on the multistep hydrodeoxygenation (HDO) of acetone (CH_3COCH_3) to propylene (CH_3CHCH_2) on a molybdenum oxide (α-MoO_3) catalyst following an oxygen vacancy-driven pathway. First, a perfect O-terminated α-MoO_3 (010) surface based on a 4 × 2 × 4 supercell is reduced by molecular hydrogen (H_2) to generate a terminal oxygen (O_t) defect site. This process occurs via a dissociative chemisorption of H_2 on adjacent surface oxygen atoms, followed by an H transfer to form a water molecule (H_2O). Next, adsorption of CH_3COCH_3 on the oxygen-deficient Mo site forms an O−Mo bond and then the chemisorbed CH_3COCH_3 forms CH_3COCH_2 by transfer of an H atom to an adjacent O_t site. The surface bound hydroxyl (OH) then transfers the H atom to the immobilized O atom to form surface-bound enol, CH_3CHOCH_2. The next step releases CH_3CHCH_2 into the gas phase, while simultaneously oxidizes the surface back to a perfect O-terminated α-MoO_3 (010) surface. The adsorption of H_2, and the formation of a terminal oxygen (O_t) vacancy, moves the conduction band minimum (CBM) from 1.2 eV to 0 and 0.3 eV, respectively. Climbing image-nudged elastic band (CI-NEB) calculations using a Perdew−Burke−Ernzerhof (PBE) functional in combination with double-ζ valence (DZV) basis sets indicate that the dissociative adsorption of H_2 is the rate-limiting step for the catalytic cycle with a barrier of 1.70 eV. Furthermore, the lower barrier for surface-mediated H transfer from primary-to-secondary carbon atom (0.63 eV) compared to that of a concerted direct H transfer to the secondary C atom with simultaneous desorption (2.02 eV) emphasizes the key role played by the surface in H transfer for effective deoxygenation.

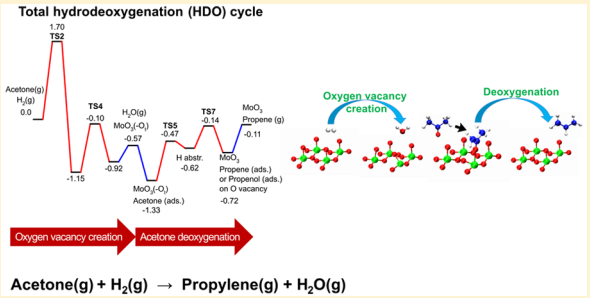

1. INTRODUCTION

Hydrodeoxygenation (HDO) is one of the most promising catalytic routes for upgrading biomass-derived pyrolysis oils into transportation fuels.[1,2] Bio-oil contains large amounts of oxygenates, including carboxylic acids, aldehydes, and ketones, which make it unsuitable for use in a transportation fuel without upgrading.[3,4] Catalytic upgrading strategies with conventional industrial hydrotreating or noble metal catalysts face many disadvantages, including significant H_2 consumption associated with saturating the highly prevalent C=C bonds (including aromatics) in bio-oil.[5] Furthermore, the high H_2 pressure used in this process leads to high capital costs.[6] Hence, optimal bio-oil upgrading processes would ideally use catalysts that selectively cleave C−O bonds using low H_2 pressures. Recently, Prasomsri et al. demonstrated that several reducible metal oxides, including α-MoO_3, are effective HDO catalysts capable of selectively cleaving C−O bonds in various bio-oil derived oxygenates under mild reaction conditions.[7] It was hypothesized that the reaction occurs via an oxygen-vacancy driven mechanism, wherein the reducing conditions promote oxygen removal from the oxide lattice, generating highly oxophilic vacancy sites. In these undercoordinated sites, oxygenates can preferentially adsorb and undergo selective C−O bond cleavage releasing a deoxygenated hydrocarbon molecule and replenishing the oxygen vacancy at the surface.

Most computational investigations on α-MoO_3 have focused on the thermodynamics of oxygen-vacancy formation on its most stable (010) surface.[8−14] Kim et al. established the link between oxygen vacancies on α-MoO_3 and its improved electrochemical properties.[15] Recently, a few studies have further detailed the elementary steps involved in the oxygen vacancy formation.[16,17] While for oxidation reactions, computational studies have focused on the oxidation of reactants by lattice oxygen of α-MoO_3,[18−20] only a few reports have studied hydrodeoxygenation (HDO) reactions on the oxophilic vacancy sites.[16,17] Furthermore, most studies were carried on cluster models, which are not representative of the (010) surface.[8,10,12,16] For new and improved catalyst design for HDO of bio-oil and other biomass-derived molecules,[21] it is important to obtain a fundamental understanding on the thermodynamics and kinetics of the elementary steps involved in the oxygen-vacancy formation and subsequent deoxygenation steps during the HDO cycle. Recently, Mei et al. utilized periodic slab calculations on a 2 × 1 × 2 supercell to investigate oxygen vacancy formation on the α-MoO_3 (010) surface and HDO of acetaldehyde (CH_3CHO) on the oxygen vacancy.[17]

Received: March 28, 2017
Revised: July 20, 2017
Published: July 25, 2017

DOI: 10.1021/acs.jpcc.7b02942
J. Phys. Chem. C 2017, 121, 17848−17855

Further, Grabow and co-workers explored pathways for oxygen vacancy formation and HDO of furan on the α-MoO_3 (010) surface.[22] Except for these studies, no other DFT calculations on periodic slab models have focused on the combined thermodynamics and kinetics during the elementary steps of HDO.[17] While the dissociative H_2 adsorption was assumed to occur without any activation barrier, the bond dissociation energy of a H_2 molecule is high (4.5 eV at 298 K),[23] and its adsorption may likely occur with a high barrier, akin to H_2 adsorption on MoS_2.[24] In addition, the computations were performed for a slab with a moderate oxygen vacancy concentration (~25% of all terminal oxygen atoms removed) and does not likely represent the reaction conditions at the HDO initiation stage or low surface oxygen vacancy concentrations (~5%) at typical HDO reaction conditions (573−673 K, ~100 kPa H_2) as reported by Prasomsri et al.[7] and Moberg et al.[16] Furthermore, the impact of oxygen vacancy formation on the electronic structure was not studied.

Acetone is one of the simplest oxygenate molecules that can be used as a model reactant to study the HDO reaction on an O-terminated α-MoO_3 (010) surface. Prasomsri et al. demonstrated propylene as the dominant product from the HDO of acetone on α-MoO_3.[7] As such, herein we report periodic ab initio density functional theory (DFT) calculations on the HDO cycle for acetone (CH_3COCH_3) conversion to propylene (CH_3CHCH_2) using a α-MoO_3 (010) 4 × 2 × 4 supercell. We report the energies and the activation energy barriers for the different elementary steps involved with the HDO catalytic cycle at low oxygen vacancy concentrations (~6% of all terminal oxygen atoms removed). In addition, the impact of H_2 adsorption and oxygen vacancy formation on the electronic structure was studied.

2. COMPUTATIONAL DETAILS

α-MoO_3 is the stable and most common crystalline phase of MoO_3.[17] All ab initio density functional theory (DFT) calculations were carried out using the Gaussian and Plane Wave approach and QUICKSTEP algorithm, implemented in the CP2K software package[25] (version 2.6.1) on HOPPER and Cori at the National Energy Research Scientific Computing Center (NERSC). The generalized gradient (GGA) corrected Perdew−Burke−Ernzerhof (PBE) exchange correlation functional[26] was used in combination with the double-ζ valence (DZV) basis sets optimized from molecular calculations. The plane-wave cutoff energy was 300 Ry at the finest level of the multigrid with a total of 4 multigrids. The cutoff energy used for the Gaussian is 40 Ry. Goedecker-Teter-Hutter (GTH) pseudopotentials[27,28] were used with 1, 4, 6, and 14 valence electrons for H, C, O, and Mo, respectively. The geometry optimizations were performed on both spin-restricted and spin-polarized basis. The difference in the computed energies was within ±0.15 eV (Figure S1). A three-dimensional periodic bulk supercell of 4 × 2 × 4 unit cells of α-MoO_3 (Figure 1) was optimized to obtain the relaxed cell parameters with angles fixed at experimental values.[29] An oxygen-terminated [010] surface slab was created using the computed bulk geometry, and the slab geometry was then relaxed with the bottom layer of MoO_3 groups fixed in their positions, resulting in 6 free layers of MoO_3 groups. A vacuum space of 12 Å was added to separate the periodic slabs along the [010] direction. The geometry and cell optimizations were considered to have converged if the maximum and root-mean-square (RMS) geometry changes per iteration were below 0.0016 and 0.0008 Å and the maximum and RMS force acting on each atom were below 0.024 and 0.016 eV $Å^{-1}$, respectively. The density of states (DOS) were projected by adding 100 virtual orbitals to the molecular orbitals.

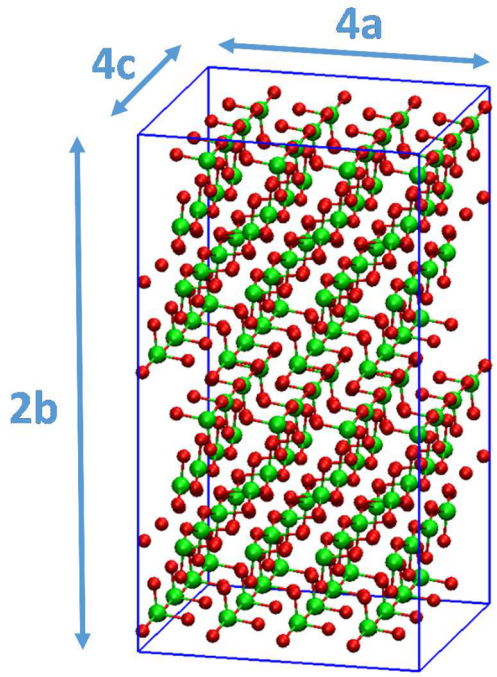

Figure 1. Optimized α-MoO_3 supercell with a = 3.961, b = 14.611, and c = 3.683 Å; Mo and O atoms are shown in green and red colors, respectively.

Following common practice, the adsorption energy (E_{ad}) of an adsorbate on the α-MoO_3 (010) surface was calculated as shown in eq 1 below:

$$E_{ad} = E_{adsorbate-surface} - (E_{surface} + E_{adsorbate}) \quad (1)$$

where $E_{adsorbate-surface}$ is the total energy of the system with geometry-optimized adsorbate on the surface, $E_{surface}$ is the total energy of the optimized $Mo_{112}O_{336}$ slab, and $E_{adsorbate}$ is the total energy of acetone (CH_3COCH_3), propylene (CH_3CHCH_2), H_2, or H_2O molecules computed in a periodic cubic vacuum box of edge-length 15 Å. The vacancy formation energies were computed using triplet O_2 and H_2O as references. As DFT methods are known to be inadequate for determining the energy of triplet O_2, because of its unpaired electrons,[30] the energy of formation of H_2O was used as a reference for the oxygen vacancy formation energies, following the method used by Rossmeisl et al.[30] Note that eq 1 does not account for changes in zero-point energies (ZPE) or heat capacities, since computing those second-order effects would require expensive second-derivative calculations. The computed DFT energetics also do not account for temperature, pressure, entropy, or coverage effects.

The minimum energy paths (MEP) and the activation energy barriers for all the elementary steps were computed using the climbing image nudged elastic band (CI-NEB) method.[31,32] MEP for each elementary step was discretized using 6−10 images as initial guesses. The convergence criteria were 0.0016 and 0.0003 Å for the maximum and RMS displacement on the band, respectively, and 0.051 and 0.026 eV $Å^{-1}$ for the maximum and RMS force on the band, respectively. These convergence limits are comparable to those used in the study

DOI: 10.1021/acs.jpcc.7b02942
J. Phys. Chem. C 2017, 121, 17848−17855

by Mei et al.[17] All the NEB calculations were spin-restricted. Since the difference in computed energies for the intermediates between spin-restricted and spin-polarized calculations were within ±0.15 eV, spin-polarized single-point energy calculations were performed for the transition state geometries identified with spin-restricted calculations, similar to Nørskov and co-workers.[33] The difference in the energy values for the transition states was negligible.

3. RESULTS

3.1. Geometry and Electronic Properties of Bulk α-MoO_3 and α- MoO_3 (010) Surface. The optimized bulk lattice parameters for the 4 × 2 × 4 supercell are a = 3.961, b = 14.611, and c = 3.683 Å. These values are in overall good agreement with experimental lattice constant values (Table 1).[29] The calculated lattice constant b is slightly longer, as α-MoO_3 slabs along [010] direction are packed via van der Waals interactions and GGA methods underestimate such interactions.[34] As shown in Figure 2a, there exist 3 different oxygen sites on the surface of α-MoO_3, a single-coordinate terminal oxygen atom (O_t), a two-coordinate asymmetric bridging oxygen atom (O_{as}), and a three-coordinate symmetric bridging oxygen atom (O_s). The bond lengths for the three Mo−O bonds are shown in Table 2. The Mo−O_t bond length is 1.68 Å, which is smaller than both symmetric Mo−O_s (1.95 Å) and asymmetric Mo−O_{as} bond lengths (1.75 and 2.23 Å). On the (010) surface, these bond lengths did not show any significant change. O_{as} lies in almost the same plane as Mo atoms, as seen by the Mo−O_{as}-Mo bond angle of 190.0° between adjacent Mo atoms (Figure 2a). The covalent interactions within the bilayers are accurately represented in the calculations, as the bond length values are consistent with both experiments and previous DFT calculations.[8,35−37]

Table 1. Calculated (PBE) Lattice Constants of α-MoO_3 4 × 2 × 4 supercell and Comparison with Experimental Lattice Constants

	lattice constants (Å)		
	A	B	c
4 × 2 × 4	3.961	14.611	3.683
Exptl.[29]	3.963	13.855	3.674

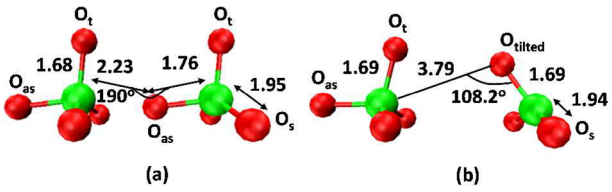

Figure 2. Mo−O bond lengths for surface layer of (a) pristine and (b) terminal oxygen (O_t) vacancy on the α-MoO_3 (010) surface. The atoms shown here exist in the top layer of the optimized α-MoO_3 (010) surface. The surface terminal (O_t), asymmetric (O_{as}), and symmetric (O_s) oxygen atoms are shown, along with the relevant Mo−O bond lengths. Mo and O are shown in green and red, respectively. O_{tilted} is a former O_{as} after creation of an O_t vacancy.

Table 2. Calculated (PBE) Mo−O Bond Lengths for Bulk α-MoO_3 and α-MoO_3 4 × 2 × 4 (010) Surface

	bond lengths (Å)	
	bulk α-MoO_3	α-MoO_3 (010) surface
Mo−O_t	1.68	1.69
Mo−O_s	1.95	1.95
Mo−O_{as}	1.75, 2.23	1.76, 2.23

The total density of states (DOS) of the periodic α-MoO_3 4 × 2 × 4 supercell presents the location of the valence band and the beginning of the conduction band (Figure S2). The calculated valence band region has a width of ∼6.5 eV, consistent with previous reports.[9,34,36,38,39] α-MoO_3 is an n-type semiconductor with an indirect band gap of 3.1 eV.[39,40] In this work, we have computed a band gap of ∼1.5 eV, consistent with previous reports.[9,38] This value is within the expected accuracy of DFT because DFT methods are known to underestimate the band gap.[9] However, we note that we are only interested in the relative values of bandgap at different steps during the reaction sequence. The conduction band minimum (CBM) was at ∼1.8 eV with respect to the Fermi level. Upon the creation of an O-terminated α-MoO_3 (010) surface, the calculated band gap reduces from 1.5 to 1.2 eV, which is also the location of CBM with respect to the Fermi level. The width of the valence band increases to ∼6.8 eV. This effect is likely caused as the electrons from the under-coordinated surface O_t atoms occupy the CBM and/or the VBM.[36]

3.2. Oxygen Vacancy Creation on α-MoO_3 (010) Surface. An oxygen vacancy can be formed by extracting any of the three types of surface oxygen atoms. Previous reports have shown that the creation of an oxygen vacancy at the O_s site is energetically unfavorable,[9,17] while the formation of an oxygen vacancy at the O_t site is energetically most favorable.[41,42] Further, the transformation of O_s and O_{as} vacancies to O_t vacancies has been shown to be barrierless.[43] Hence, even if an O_s or O_{as} vacancy is formed, it likely spontaneously transforms into an O_t vacancy by displacement of an O_t to the O_{as} or O_s site.[43] Hence, for the current study, we will focus on the O_t vacancy formation. The formation of a terminal O_t vacancy leads to restructuring of the surface as seen in Figure 2b. The asymmetric oxygen atom (O_{as}) restructures to form a tilted terminal oxygen (O_{tilted}) atom with a Mo−O_{tilted} bond length of 1.69 Å, close to the Mo−O_t bond length on a perfect surface (Table 3). The Mo−O_{tilted}(O_{as})−Mo bond angle decreases from 190.0° to 108.2°, closer to a Mo−O_t−Mo bond angle of 62.3° for a perfect surface (Figure 2b). The surface restructures along the [001] direction, and the O_s atom gets displaced by a small value with the two Mo−O_s bond lengths at 1.94 and 1.97 Å (Table 3). The distances between

Table 3. Calculated Bond Lengths and Bond Angles on α-MoO_3 4 × 2 × 4 (010) Perfect Surface and Surface with Single Terminal Oxygen (O_t) Vacancy

	bond lengths (Å)/bond angles	
	perfect surface	surface with single O_t vacancy
Mo−O_t[a]	1.69	1.69
Mo−O_s	1.95	1.97, 1.94
Mo−O_{as}	1.76, 2.23	1.79, 2.02
Mo−O_{as}−Mo	190°	108.2°

[a]For the surface with single terminal oxygen (O_t) vacancy, O_t corresponds to the tilted oxygen atom (O_{tilted}) as shown in Figure 2b.

DOI: 10.1021/acs.jpcc.7b02942
J. Phys. Chem. C 2017, 121, 17848−17855

O_{tilted} and the nearest fully coordinated Mo atoms are 3.79 and 3.90 Å.

In this study, we have calculated a terminal O_t vacancy formation energy of 2.40 eV, with molecular triplet O_2 as a reference (Table S1), which are in qualitative agreement with other DFT calculations on clusters and surfaces.[8−10,16,17] We note that the vacancy formation energy is high, therefore at HDO operating conditions (T = 573−673 K), a reducing atmosphere (e.g., ∼100 kPa H_2) helps in the formation of oxygen vacancies, aided by the formation of H_2O from the combination of a terminal oxygen (O_t) with H_2.[7,44]

For a surface with a single terminal oxygen (O_t) vacancy in each supercell [i.e., 1/16th (∼6%) of total O_t's removed], our calculations show that the CBM approaches the Fermi level with its location 0.3 eV above the Fermi level (Figure 3). Even

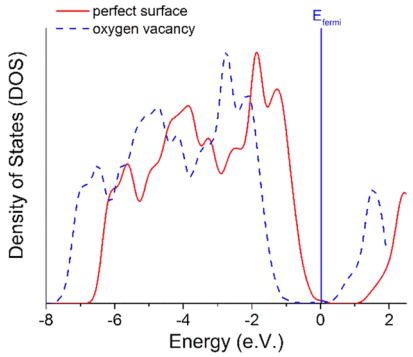

Figure 3. Calculated density of states (DOS) for perfect α-MoO_3 (010) surface and α-MoO_3 (010) surface with a single terminal oxygen (O_t) vacancy for 4 × 2 × 4 supercell.

though the band gap is underestimated in DFT, we note that an α-MoO_3 (010) surface approaches metallic behavior after O_t vacancy creation, as seen by the drastic reduction in the location of CBM. The valence bandwidth is ∼6.8 eV, and the band gap reduces to ∼1 eV, suggesting that the electrons post vacancy-creation occupy the CBM and/or VBM.

3.3. Facilitated Oxygen Vacancy Formation in the Presence of H_2. In a reducing H_2 atmosphere, the dissociative adsorption of H_2 can occur on surface oxygen atoms of α-MoO_3 (010) surface to form surface hydroxyls. Here, two likely configurations of surface hydroxyls on dissociative H_2 adsorption were explored: two terminal hydroxyls (2 O_tH) and two surface hydroxyls at asymmetric and terminal oxygen sites ($O_{as}H$ and O_tH). The relevant bond lengths are detailed in the Supporting Information (S.1). The configuration with O_tH and $O_{as}H$ was computed to be energetically favorable, consistent with the results by Mei et al.[17] This is similar to the formation of $O_{as}H$ as the energetically favorable configuration for atomic H adsorption (Table 4), in contrast with recent reports[16,17,34,45] but consistent with a recent report by Grabow and co-workers.[22] The geometries are in given in the Supporting Information (S.2.). The surface hydroxyls can

Table 4. Atomic H Adsorption Energies at Terminal, Asymmetric, and Symmetric Oxygen

	adsorption energy (eV)
O_tH	−0.33
O_sH	−0.31
$O_{as}H$	−0.87

then combine to form a H_2O molecule bound on a Mo site (Figure 4). This surface reconstruction causes an asymmetric O_{as} to tilt out of plane (Figure 4). Our calculations show that the dissociative adsorption of H_2 to form O_tHs occurs with a higher barrier (2.16 eV, TS1) than that for the formation of $O_{as}H$ and O_tH (1.70 eV, TS2), as shown in Figure 4. The combination of surface hydroxyls to form a water molecule has a lower barrier for the combination of two O_tH hydroxyls (0.41 eV, TS3) than for the recombination of $O_{as}H$ and O_tH hydroxyls (1.05 eV, TS4). Finally, the water desorption is barrierless with a desorption energy of 0.35 eV, leaving an O_t vacancy on the surface. The geometries for the transition states and final states are given in Figure 4 and Supporting Information (S.3 and S.4).

Our calculations show that as compared to a vacancy formation energy of +2.40 eV to form triplet O_2, the total process of oxygen vacancy formation by reaction with H_2 to form H_2O is exothermic with a total reaction enthalpy of −0.57 eV (Table S1) but with a kinetic barrier of +1.70 eV (Figure 4). Taken together, these data show that oxygen vacancy formation is significantly facilitated and enhanced in the presence of H_2, albeit with a high kinetic barrier.

Akin to the case of oxygen vacancy formation, the CBM is located at the Fermi level on adsorption of hydrogen on the oxygen-terminated surface for configurations involving two surface hydroxyls ($O_{as}H$ and O_tH) and the case of an adsorbed water molecule (Figure S11). The band gap is reduced to ∼0.8 eV. Such a decrease in band gap and the approach of α-MoO_3 (010) surface to metallic behavior has been previously reported for hydrogen adsorption/intercalation on the α-MoO_3 (010) surface.[34,46,47]

3.4. Elementary Steps for Conversion of Acetone to Propylene. The elementary steps for CH_3COCH_3 adsorption and further conversion to propylene (CH_3CHCH_2) were investigated on a α-MoO_3 (010) surface containing a single terminal oxygen (O_t) vacancy (Figure 5). On a surface with a terminal O_t defect, CH_3COCH_3 adsorption is barrierless, featuring a computed binding energy of −0.76 eV. The details of the geometry are given in the Supporting Information (S.5.). The elementary steps for conversion of CH_3COCH_3 to CH_3CHCH_2 involve transfer of an H atom from a terminal primary carbon atom to the central carbon atom followed by cleavage of the C═O bond. Two likely conversion pathways are explored after H transfer from a terminal carbon atom to surface oxygen: (1) a concerted H migration and C−O cleavage with simultaneous desorption of propylene (TS6) and (2) a two-step process with H transfer and C−O cleavage to form adsorbed propylene, followed by propylene desorption (TS7). Both hydrodeoxygenation sequences end with a fully oxidized α-MoO_3 (010) surface.

The H migration can occur from one of the two identical terminal methyl (CH_3) groups. The H abstraction to an adjacent O_t atom is endothermic with a reaction energy of 0.70 eV and a reaction barrier of 1.0 eV (TS5). For the concerted pathway, the subsequent step involves the transfer of H from an adjacent O_t atom to the central carbon atom. This step is endothermic with a reaction energy 0.51 eV and a reaction barrier of 2.02 eV. The high barrier makes this pathway unfavorable. In the two-step pathway, CH_3CHCH_2 is formed in an adsorbed configuration prior to desorbing. Note that the adsorbed propylene resembles the configuration of propenol adsorbed on a terminal oxygen (O_t) vacancy. The formation of propylene in an adsorbed configuration (propenol adsorbed on

DOI: 10.1021/acs.jpcc.7b02942
J. Phys. Chem. C 2017, 121, 17848−17855

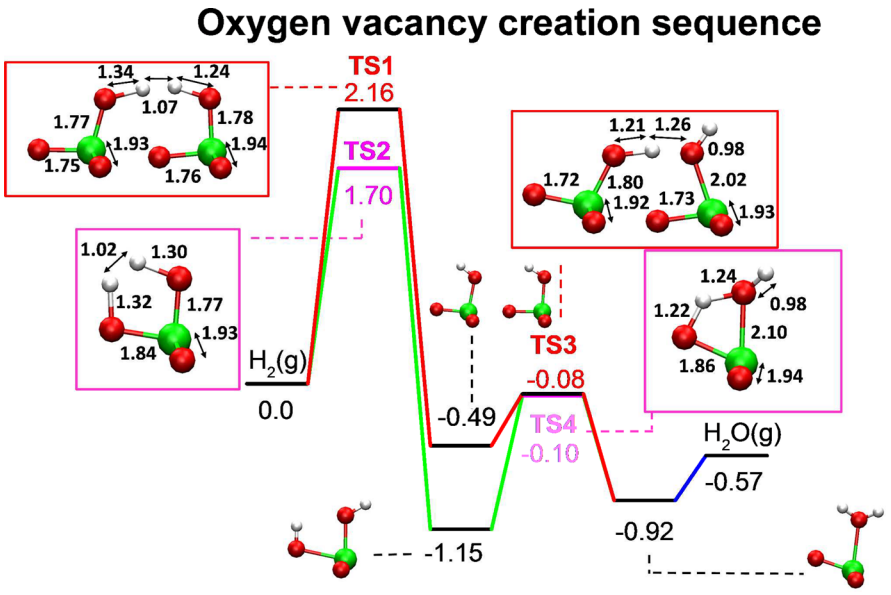

Figure 4. Reaction coordinate for formation of oxygen vacancy through H_2O formation on an O terminated α-MoO_3 (010) surface. Mo, O, and H are shown in green, red, and white, respectively. All energies are in eV.

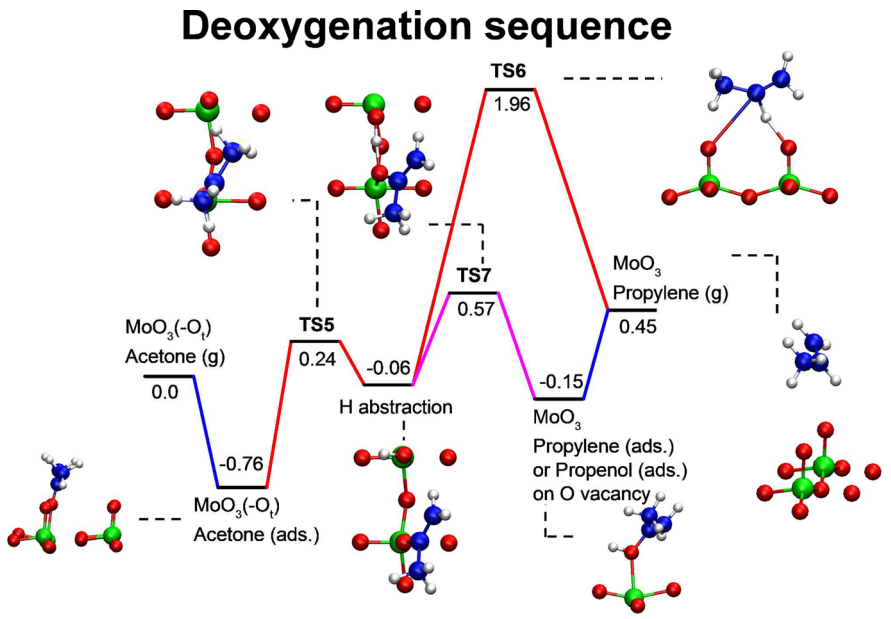

Figure 5. Reaction coordinate for acetone deoxygenation to propylene on α-MoO_3 (010) surface with a single terminal (O_t) vacancy. Mo, O, C, and H are shown in green, red, blue, and white, respectively. All energies are in eV.

an oxygen vacancy) occurs with −0.09 eV change in energy and a barrier of 0.63 eV. Due to the lower barrier, deoxygenation likely follows this pathway. We note that our computations suggest that propylene reacts barrierlessly with the surface to form chemisorbed propenol (on an oxygen vacancy). In the final state, propylene is desorbed from the surface with a desorption energy of 0.60 eV. The geometries of the intermediate and transition states are given in the Supporting Information (S.6.).

4. DISCUSSION

Overall, the potential energy surface (PES) shows two competitive paths each for oxygen vacancy creation (Figure 4) and acetone deoxygenation (Figure 5). For oxygen vacancy creation, prior researchers concluded that vacancy formation on an O-terminated α-MoO_3 (010) surface was fast.[16,17] However, the barriers involved in the H_2 chemisorption step were not computed. Our work shows that this step could indeed be rate-limiting. We note that this result is consistent with the recent work by Grabow and co-workers.[22] Hence, Pt is often used as a dopant on MoO_3 catalysts to accelerate H_2 splitting and reduction of MoO_3.[48,49] Because the barriers associated with dissociative H_2 chemisorption is high, the HDO rate is likely to be H_2 pressure-dependent, consistent with experimental observations on bulk α-MoO_3.[7] Further, the presence of coordinatively unsaturated metal sites can significantly reduce the barriers associated with oxygen vacancy formation, as shown by Vlachos and co-workers on RuO_2 (110) surface.[50] Our results suggest that alternate mechanisms for oxygen vacancy creation may need to be explored, including the effect

DOI: 10.1021/acs.jpcc.7b02942
J. Phys. Chem. C 2017, 121, 17848−17855

of coordinatively unsaturated Mo species on the H_2 adsorption mechanism. For the acetone deoxygenation part of the cycle, our results show that surface-mediated hydrogen transfer during deoxygenation to surface propyl has a lower barrier than an alternate pathway involving concerted desorption and hydrogen migration. Figure 6 shows the reaction route with the

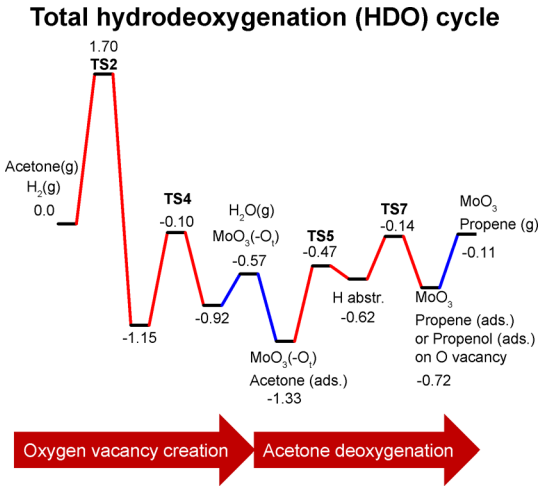

Figure 6. Total HDO pathway for CH_3COCH_3 (acetone) + H_2 (hydrogen) → CH_3CHCH_2 (propylene) + H_2O (water). All energies are in eV.

smallest activation energy barriers during different elementary steps. Our results suggest that at low oxygen vacancy (~6% of all terminal oxygen atoms removed) concentration, acetone deoxygenation on an oxygen vacancy is relatively facile. Overall, the cycle is mildly exothermic with total energy −0.11 eV.

Our study considers a phase-pure α-MoO_3 (010) surface which represents the initial state of the catalyst. At many reaction conditions, the catalyst is partially reduced and carburized to an oxycarbidic phase ($MoO_xC_yH_z$).[44] Consequently, the experimental reaction kinetics for HDO on phase-pure α-MoO_3 is difficult to obtain. It may be insightful to study the effect of the phase-change on the barriers associated with the reaction pathway. Our DOS calculations suggest that α-MoO_3 (010) surface approaches metallic character on an oxygen vacancy creation. Typically, materials demonstrating metallic character and defect sites have been shown to exhibit relatively facile H_2 dissociative adsorption.[51−54] The barriers associated with dissociative H_2 chemisorption might plausibly reduce on creation of oxygen vacancies due to the formation on undercoordinated Mo sites and the metallic nature of the surface. Recently, Shetty et al. established higher HDO reactivity, for *m*-cresol conversion to toluene, for MoO_3 supported on TiO_2 and ZrO_2 than bulk α-MoO_3, which correlated with the reducibility (obtained by H_2 temperature programed reduction) of dispersed MoO_3 species on these supports.[55] Similar support effects were also observed for a number of other redox reactions.[56−58] This suggests that the Mo−O bond strengths and propensity for oxygen vacancy creation varies across different supports. Furthermore, the speciation of MoO_x species influenced its reducibility and reactivity toward HDO reactivity.[59] Additional computational investigations could provide valuable insights into the genesis of the support effect on vacancy creation and HDO reactivity. Finally, a better idea on the accuracy of the methods can be understood by understanding the effect of the choice of methods and functionals, including the use of DFT+U methods, hybrid functionals, and van der Waals interactions on the energies of intermediates and the transition states (especially the H_2 dissociation barriers).

5. CONCLUSIONS

The elementary steps for hydrodeoxygenation (HDO) of acetone to propylene on an O-terminated α-MoO_3 (010) surface have been investigated. Our calculated density of states (DOS) show that the creation of an oxygen vacancy, or hydrogen adsorption, makes the α-MoO_3 (010) surface approach metallic behavior. Further, the activation energies of the total cycle show that dissociative hydrogen adsorption could be the rate-determining step for total HDO. The surface-mediated two-step deoxygenation mechanism from acetone adsorbed on a single oxygen vacancy to form chemisorbed propylene is the most favorable deoxygenation pathway. Our results pave the way for future studies on HDO catalysts and explorations of the barrier associated with H_2 chemisorption on these materials. Detailed mechanisms, especially for the oxycarbidic phase ($MoO_xC_yH_z$) and supported MoO_3 catalysts, would be very helpful for understanding the effect of phase-modification and support on oxygen vacancy creation and HDO reactivity.

■ ASSOCIATED CONTENT

Supporting Information

The Supporting Information is available free of charge on the ACS Publications website at DOI: 10.1021/acs.jpcc.7b02942.

Structural information on the optimized initial and transition states of the elementary steps along with the density of states (DOS) for adsorbed H configurations are provided (PDF)

■ AUTHOR INFORMATION

Corresponding Author

*E-mail: whgreen@mit.edu. Tel: 1-617-253-4307.

ORCID

Manish Shetty: 0000-0002-8611-7415
Yuriy Román-Leshkov: 0000-0002-0025-4233
William H. Green: 0000-0003-2603-9694

Present Address

†IBM Research, Dublin, Ireland.

Author Contributions

The manuscript was written through contributions of all authors. All authors have given approval to the final version of the manuscript.

Notes

The authors declare no competing financial interest.

■ ACKNOWLEDGMENTS

The authors gratefully acknowledge financial support from BP (Award 1454299). The authors would like to thank the National Energy Research Scientific Computing Center (NERSC) for computational resources (Contract DE-AC02-05CH11231). The authors would also like to acknowledge Dr. Christopher Hendon and Dr. Phalgun Lolur at the Department of Chemical Engineering, Massachusetts Institute of Technology, for valuable discussions.

DOI: 10.1021/acs.jpcc.7b02942
J. Phys. Chem. C 2017, 121, 17848−17855

REFERENCES

(1) Bu, Q.; Lei, H.; Zacher, A. H.; Wang, L.; Ren, S.; Liang, J.; Wei, Y.; Liu, Y.; Tang, J.; Zhang, Q.; Ruan, R. A Review of Catalytic Hydrodeoxygenation of Lignin-Derived Phenols from Biomass Pyrolysis. *Bioresour. Technol.* **2012**, *124*, 470−477.

(2) Saidi, M.; Samimi, F.; Karimipourfard, D.; Nimmanwudipong, T.; Gates, B. C.; Rahimpour, M. R. Upgrading of Lignin-Derived Bio-Oils by Catalytic Hydrodeoxygenation. *Energy Environ. Sci.* **2014**, *7*, 103−129.

(3) Czernik, S.; Bridgwater, A. V. Overview of Applications of Biomass Fast Pyrolysis Oil. *Energy Fuels* **2004**, *18*, 590−598.

(4) Zhang, Q.; Chang, J.; Wang, T.; Xu, Y. Review of Biomass Pyrolysis Oil Properties and Upgrading Research. *Energy Convers. Manage.* **2007**, *48*, 87−92.

(5) Huber, G. W.; Iborra, S.; Corma, A. Synthesis of Transportation Fuels from Biomass: Chemistry, Catalysts, and Engineering. *Chem. Rev.* **2006**, *106*, 4044−4098.

(6) Simbeck, D.; Chang, E. *Hydrogen Supply: Cost Estimate for Hydrogen Pathways−Scoping Analysis*; NREL: Golden, CO, 2002.

(7) Prasomsri, T.; Nimmanwudipong, T.; Roman-Leshkov, Y. Effective Hydrodeoxygenation of Biomass-Derived Oxygenates into Unsaturated Hydrocarbons by MoO3 Using Low H2 Pressures. *Energy Environ. Sci.* **2013**, *6*, 1732−1738.

(8) Tokarz-Sobieraj, R.; Hermann, K.; Witko, M.; Blume, A.; Mestl, G.; Schlogl, R. Properties of Oxygen Sites at the MoO3(010) Surface: Density Functional Theory Cluster Studies and Photoemission Experiments. *Surf. Sci.* **2001**, *489*, 107−125.

(9) Coquet, R.; Willock, D. J. The (010) Surface of Alpha-MoO3, a DFT+U Study. *Phys. Chem. Chem. Phys.* **2005**, *7*, 3819−3828.

(10) Tokarz-Sobieraj, R.; Witko, M.; Grybos, R. Reduction and Re-Oxidation of Molybdena and Vanadia: DFT Cluster Model Studies. *Catal. Today* **2005**, *99*, 241−253.

(11) Lei, Y. H.; Chen, Z. X. DFT+U Study of Properties of MoO3 and Hydrogen Adsorption on MoO3(010). *J. Phys. Chem. C* **2012**, *116*, 25757−25764.

(12) Witko, M.; Tokarz-Sobieraj, R. Surface Oxygen in Catalysts Based on Transition Metal Oxides: What Can We Learn from Cluster DFT Calculations? *Catal. Today* **2004**, *91−92*, 171−176.

(13) Inzani, K.; Grande, T.; Vullum-Bruer, F.; Selbach, S. M. A Van Der Waals Density Functional Study of MoO3 and Its Oxygen Vacancies. *J. Phys. Chem. C* **2016**, *120*, 8959−8968.

(14) Agarwal, V.; Metiu, H. Oxygen Vacancy Formation on α-MoO3 Slabs and Ribbons. *J. Phys. Chem. C* **2016**, *120*, 19252−19264.

(15) Kim, H.-S.; Cook, J. B.; Lin, H.; Ko, J. S.; Tolbert, S. H.; Ozolins, V.; Dunn, B. Oxygen Vacancies Enhance Pseudocapacitive Charge Storage Properties of MoO3-x. *Nat. Mater.* **2016**, *16*, 454−460.

(16) Moberg, D. R.; Thibodeau, T. J.; Amar, F. o. G.; Frederick, B. G. Mechanism of Hydrodeoxygenation of Acrolein on a Cluster Model of MoO3. *J. Phys. Chem. C* **2010**, *114*, 13782−13795.

(17) Mei, D.; Karim, A. M.; Wang, Y. Density Functional Theory Study of Acetaldehyde Hydrodeoxygenation on MoO3. *J. Phys. Chem. C* **2011**, *115*, 8155−8164.

(18) Fu, G.; Xu, X.; Lu, X.; Wan, H. L. Mechanisms of Initial Propane Activation on Molybdenum Oxides: A Density Functional Theory Study. *J. Phys. Chem. B* **2005**, *109*, 6416−6421.

(19) Rappe, A. K.; Goddard, W. A. Hydrocarbon Oxidation by High-Valent Group VI Oxides. *J. Am. Chem. Soc.* **1982**, *104*, 3287−3294.

(20) Choksi, T.; Greeley, J. Partial Oxidation of Methanol on MoO3 (010): A DFT and Microkinetic Study. *ACS Catal.* **2016**, *6*, 7260−7277.

(21) Anderson, E. M.; Katahira, R.; Reed, M.; Resch, M. G.; Karp, E. M.; Beckham, G. T.; Román-Leshkov, Y. Reductive Catalytic Fractionation of Corn Stover Lignin. *ACS Sustainable Chem. Eng.* **2016**, *4*, 6940−6950.

(22) Kasiraju, S.; Grabow, L. *Hydrodeoxygenation of Furan on Oxygen Vacancy Sites of MoO3(010): A DFT Investigation*, 250th National Meeting of the American Chemical Society, Boston, Massachusetts, Aug 16−20, 2015; American Chemical Society: Washington, DC, 2015.

(23) Herzberg, G.; Monfils, A. The Dissociation Energies of the H2, HD, and D2 Molecules. *J. Mol. Spectrosc.* **1961**, *5*, 482−498.

(24) Sun, M. Y.; Nelson, A. E.; Adjaye, J. Ab Initio DFT Study of Hydrogen Dissociation on MoS2, NiMoS, and CoMoS: Mechanism, Kinetics, and Vibrational Frequencies. *J. Catal.* **2005**, *233*, 411−421.

(25) Hutter, J.; Iannuzzi, M.; Schiffmann, F.; VandeVoldele, J. CP2K; atomistic simulations of condensed matter systems. *J. Wires. Comput. Mol. Sci.* **2014**, *4*, 15.

(26) Perdew, J. P.; Burke, K.; Ernzerhof, M. Generalized Gradient Approximation Made Simple. *Phys. Rev. Lett.* **1996**, *77*, 3865−3868.

(27) Goedecker, S.; Teter, M.; Hutter, J. Separable Dual-Space Gaussian Pseudopotentials. *Phys. Rev. B: Condens. Matter Mater. Phys.* **1996**, *54*, 1703−1710.

(28) Hartwigsen, C.; Goedecker, S.; Hutter, J. Relativistic Separable Dual-Space Gaussian Pseudopotentials from H to Rn. *Phys. Rev. B: Condens. Matter Mater. Phys.* **1998**, *58*, 3641−3662.

(29) Andersson, G.; Magneli, A.; Sillén, L. G.; Rottenberg, M. On the Crystal Structure of Molybdenum Trioxide. *Acta Chem. Scand.* **1950**, *4*, 793−797.

(30) Rossmeisl, J.; Logadottir, A.; Nørskov, J. K. Electrolysis of Water on (Oxidized) Metal Surfaces. *Chem. Phys.* **2005**, *319*, 178−184.

(31) Henkelman, G.; Jonsson, H. Improved Tangent Estimate in the Nudged Elastic Band Method for Finding Minimum Energy Paths and Saddle Points. *J. Chem. Phys.* **2000**, *113*, 9978−9985.

(32) Henkelman, G.; Uberuaga, B. P.; Jonsson, H. A Climbing Image Nudged Elastic Band Method for Finding Saddle Points and Minimum Energy Paths. *J. Chem. Phys.* **2000**, *113*, 9901−9904.

(33) Studt, F.; Abild-Pedersen, F.; Varley, J. B.; Norskov, J. K. CO and CO2 Hydrogenation to Methanol Calculated Using the BEEF-Vdw Functional. *Catal. Lett.* **2013**, *143*, 71−73.

(34) Sha, X. W.; Chen, L.; Cooper, A. C.; Pez, G. P.; Cheng, H. S. Hydrogen Absorption and Diffusion in Bulk Alpha-MoO3. *J. Phys. Chem. C* **2009**, *113*, 11399−11407.

(35) Kihlborg, L. Least Squares Refinement of Crystal Structure of Molybdenum Trioxide. *Ark. Kemi* **1963**, *21*, 357−364.

(36) Huang, P. R.; He, Y.; Cao, C.; Lu, Z. H. Impact of Lattice Distortion and Electron Doping on Alpha-MoO3 Electronic Structure. *Sci. Rep.* **2015**, *4*, 10.1038/srep07131.

(37) Rutkowska-Zbik, D.; Grybos, R.; Tokarz-Sobieraj, R. DFT Investigation of Molybdenum (Oxo)Carbide Formation from MoO3. *Struct. Chem.* **2012**, *23*, 1417−1424.

(38) Scanlon, D. O.; Watson, G. W.; Payne, D. J.; Atkinson, G. R.; Egdell, R. G.; Law, D. S. L. Theoretical and Experimental Study of the Electronic Structures of MoO3 and MoO2. *J. Phys. Chem. C* **2010**, *114*, 4636−4645.

(39) Reshak, A. H. Specific Features of Electronic Structures and Optical Susceptibilities of Molybdenum Oxide. *RSC Adv.* **2015**, *5*, 22044−22052.

(40) Nirupama, V.; Gunasekhar, K. R.; Sreedhar, B.; Uthanna, S. Effect of Oxygen Partial Pressure on the Structural and Optical Properties of DC Reactive Magnetron Sputtered Molybdenum Oxide Films. *Curr. Appl. Phys.* **2010**, *10*, 272−278.

(41) Chen, M.; Friend, C. M.; Kaxiras, E. The Chemical Nature of Surface Point Defects on MoO3(010): Adsorption of Hydrogen and Methyl. *J. Am. Chem. Soc.* **2001**, *123*, 2224−2230.

(42) O'Brien, M. G.; Beale, A. M.; Jacques, S. D. M.; Buslaps, T.; Honkimaki, V.; Weckhuysen, B. M. On the Active Oxygen in Bulk MoO3 During the Anaerobic Dehydrogenation of Methanol. *J. Phys. Chem. C* **2009**, *113*, 4890−4897.

(43) Lei, Y. H.; Chen, Z. X. A Theoretical Study of Stability and Vacancy Replenishing of MoO3(0 1 0) Surfaces in Oxygen Atmosphere. *Appl. Surf. Sci.* **2016**, *361*, 107−113.

(44) Prasomsri, T.; Shetty, M.; Murugappan, K.; Román-Leshkov, Y. Insights into the Catalytic Activity and Surface Modification of MoO3 During the Hydrodeoxygenation of Lignin-Derived Model Compounds into Aromatic Hydrocarbons under Low Hydrogen Pressures. *Energy Environ. Sci.* **2014**, *7*, 2660−2669.

(45) Chen, M.; Waghmare, U. V.; Friend, C. M.; Kaxiras, E. A Density Functional Study of Clean and Hydrogen-Covered Alpha-

DOI: 10.1021/acs.jpcc.7b02942
J. Phys. Chem. C 2017, 121, 17848−17855

MoO3(010): Electronic Structure and Surface Relaxation. *J. Chem. Phys.* **1998**, *109*, 6854−6860.
(46) Yang, M.; Han, B.; Cheng, H. First-Principles Study of Hydrogenation of Ethylene on a HxMoO3(010) Surface. *J. Phys. Chem. C* **2012**, *116*, 24630−24638.
(47) Li, F. Y.; Chen, Z. F. Tuning Electronic and Magnetic Properties of MoO3 Sheets by Cutting, Hydrogenation, and External Strain: A Computational Investigation. *Nanoscale* **2013**, *5*, 5321−5333.
(48) Matsuda, T.; Uchijima, F.; Sakagami, H.; Takahashi, N. H2-Reduction of Pt/MoO3 to MoOx with a Large Surface Area and Its Catalytic Activities for the Conversions of Heptane and Propan-2-Ol. *Phys. Chem. Chem. Phys.* **2001**, *3*, 4430−4436.
(49) Matsuda, T.; Hanai, A.; Uchijima, F.; Sakagami, H.; Takahashi, N. Formation of MoOx with a Large Surface Area by H2 Reduction of MoO3 in the Presence of Pt. *Microporous Mesoporous Mater.* **2002**, *51*, 155−164.
(50) Mironenko, A. V.; Vlachos, D. G. Conjugation-Driven "Reverse Mars−Van Krevelen"-Type Radical Mechanism for Low-Temperature C−O Bond Activation. *J. Am. Chem. Soc.* **2016**, *138*, 8104−8113.
(51) Joubert, J.; Salameh, A.; Krakoviack, V.; Delbecq, F.; Sautet, P.; Coperet, C.; Basset, J. M. Heterolytic Splitting of H2 and CH4 on Gamma-Alumina as a Structural Probe for Defect Sites. *J. Phys. Chem. B* **2006**, *110*, 23944−23950.
(52) Zhou, C. G.; Wu, J. P.; Nie, A. H.; Forrey, R. C.; Tachibana, A.; Cheng, H. S. On the Sequential Hydrogen Dissociative Chemisorption on Small Platinum Clusters: A Density Functional Theory Study. *J. Phys. Chem. C* **2007**, *111*, 12773−12778.
(53) Li, B. H.; Yim, W. L.; Zhang, Q. J.; Chen, L. A Comparative Study of Hydrogen Spillover on Pd and Pt Decorated MoO3(010) Surfaces from First Principles. *J. Phys. Chem. C* **2010**, *114*, 3052−3058.
(54) Chen, H. Y. T.; Tosoni, S.; Pacchioni, G. Hydrogen Adsorption, Dissociation, and Spillover on Ru-10 Clusters Supported on Anatase TiO2 and Tetragonal ZrO2 (101) Surfaces. *ACS Catal.* **2015**, *5*, 5486−5495.
(55) Shetty, M.; Murugappan, K.; Prasomsri, T.; Green, W. H.; Roman-Leshkov, Y. Reactivity and Stability Investigation of Supported Molybdenum Oxide Catalysts for the Hydrodeoxygenation (HDO) of m-Cresol. *J. Catal.* **2015**, *331*, 86−97.
(56) Zhang, W.; Desikan, A.; Oyama, S. T. Effect of Support in Ethanol Oxidation on Molybdenum Oxide. *J. Phys. Chem.* **1995**, *99*, 14468−14476.
(57) Cherian, M.; Gupta, R.; Rao, M. S.; Deo, G. Effect of Modifiers on the Reactivity of Cr2O3/Al2O3 and Cr2O3/TiO2 Catalysts for the Oxidative Dehydrogenation of Propane. *Catal. Lett.* **2003**, *86*, 179−189.
(58) Oyama, S. T.; Radhakrishnan, R.; Seman, M.; Kondo, J. N.; Domen, K.; Asakura, K. Control of Reactivity in C-H Bond Breaking Reactions on Oxide Catalysts: Methanol Oxidation on Supported Molybdenum Oxide. *J. Phys. Chem. B* **2003**, *107*, 1845−1852.
(59) Shetty, M.; Murugappan, K.; Green, W. H.; Roman-Leshkov, Y. Structural Properties and Reactivity Trends of Molybdenum Oxide Catalysts Supported on Zirconia for the Hydrodeoxygenation of Anisole. *ACS Sustainable Chem. Eng.* **2017**, *5*, 5293−5301.

DOI: 10.1021/acs.jpcc.7b02942
J. Phys. Chem. C 2017, 121, 17848−17855